NI

NASA Technical Memorandum 81956

USAAVRADCOM TR 81-B-1

FLUID MECHANICS MECHANISMS IN THE STALL PROCESS FOR HELICOPTERS

Warren H. Young, Jr.

March 1981

National Aeronautics and Space Administration

Langley Research Center
Hampton, Virginia 23665

FLUID MECHANICS MECHANISMS IN THE STALL PROCESS OF AIRFOILS FOR HELICOPTERS

Warren H. Young, Jr.
NASA Langley Research Center
Hampton, Virginia 23665

Abstract

Recent experimental results from airfoils in the Mach number, Reynolds number or reduced frequency ranges typical of helicopter rotor blades have identified the most influential flow mechanisms in the dynamic stall process. The roles in dynamic stall of the large shed vortex from near the leading edge, a bubble of separation near the nose to facilitate transition, and rapid forward movement of the separation point through an unsteady boundary layer are well accepted. The importance of secondary shed vortices, downstream wake action, and the flow in the separated region is generally acknowledged but poorly understood. By means of surface pressure cross-correlations and flow field measurements in static stall, several new hypotheses have been generated. It is proposed that vortex shedding may be caused by acoustic disturbances propagating forward in the lower (pressure) surface boundary layer, that wake "closure" is a misnomer, and that the shed vortex leaves a trail of vorticity that forms a turbulent free shear layer. This paper reviews the known dynamic stall flow mechanisms and assesses the potential importance of recently proposed and hypothetical flow phenomena with respect to helicopter blade aeroelastic response.

Introduction

The stall of helicopter rotor blades occurs on the retreating side of the rotor disk. The lift generated on the advancing side of the disk must be balanced by lift generated on the retreating side. The lower velocity on the retreating side (typically 0.3 to 0.5 Mach number) is compensated for by higher lift coefficients which require higher angles of attack. The angle of attack distribution is illustrated in figure 1 from reference 1. When the angle of attack required for trim does not exceed the stall angle the blade performance is described by steady aerodynamics.

When stall occurs, the blade dynamic and elastic properties become important in determining the subsequent changes in angle of attack. The aerodynamics of dynamic stall govern the aeroelastic response and can lead to a dynamic instability known as stall flutter. In describing the fluid mechanics involved in dynamic stall, the blade motions must be taken into account. The three basic structural modes that are excited by dynamic stall are the blade torsional mode, the bending (normal to the chord) mode, and the flapping mode. The excitation of these three modes is illustrated in figure 2 from Crimi's aeroelastic analysis of a two-dimensional section of a helicopter blade in reference 2. The three basic structural modes of motion, at three different frequencies, contribute to the angle of attack. The mixture of modes causes the sequence of stall and unstall occurrences to be at irregular time intervals. The structural response most important to the angle of attack is the pitching displacement. The sharp spikes in the aerodynamic pitching moment act as a series of impulses to cause pitching oscillations. The unsteady lift causes lower frequency motions due to blade bending and flapping. These two plunge motions are of secondary importance in determining the angle of attack and oscillatory structural response. The structural oscillations are usually identified as being caused by stall flutter. These oscillations cause vibrations and blade loads which often limit the flight envelope.

Unlike classical (unstalled) flutter, the oscillations due to stall flutter result from a series of large impulsive aerodynamic forces. The aerodynamic damping (negative or positive) of a dynamic stall cycle does not have enough time to significantly amplify or diminish the helicopter blade oscillations. After only a few torsional oscillations the blade has rotated to the advancing side of the disk, and the mean angle of attack is too small to sustain stall flutter. Even in a steady free stream, however, the amplitude of flutter oscillations is usually limited to 8 to 20 degrees. Stall flutter also differs from classical flutter in that the torsional and bending frequencies are not close together even though both modes contribute to the stall flutter.

Most of the dynamic stall experimental work has been for a two-dimensional airfoil section oscillating sinusoidally in pitch about the quarter-chord point. Much of this research has been done at the Aeromechanics Laboratory of USARTL (AVRADCOM) by W. J. McCroskey and associates. This work has clarified the features of dynamic stall aerodynamics up to a Mach number of 0.3. Reference 3 is an overview of this research, and the most recent results are described in reference 4. The present paper will examine several recent experimental and analytical studies against the background of this research.

The purpose of this paper is to identify the many aerodynamic physical flow mechanisms which must be modeled by a numerical solution of dynamic stall. The phenomena that control the flow during the stall portion of a dynamic stall cycle are described, and their influence on blade motion is outlined. Four mechanisms by which dynamic stall may be initiated are identified. The interaction of the flow and the helicopter structural dynamics is considered in order to assess the relative importance of the various flow phenomena to a dynamic stall

calculation. The fluid mechanics that contribute to the identified flow phenomena are summarized, and the usefulness of a model that incorporates the required fluid mechanics mechanisms is outlined.

Airfoil Upper Surface Flow

Vortex Shedding

Vortex shedding is responsible for the large excursions in the pitching moment that occur after stall. A large vortex (or series of several vortices) shed from near the leading edge of the airfoil controls the flow over the upper surface of the airfoil. A two-dimensional solution of the Navier-Stokes equations by Mehta (ref. 5) has demonstrated that the speed of downstream movement and size of this vortex (fig. 3) can be calculated for laminar flows. Definition of the movement of the vortex is particularly important in calculating dynamic, aerodynamic, and structural interactions. The shed vortex contains a region of low pressure and generates a large unsteady lift force on the airfoil. As this low pressure region moves from the leading edge to the trailing edge, large time-dependent pitching moments, which are primarily nose down, are generated on the airfoil. Because of the torsional flexibility of the helicopter blades, these pitching moments cause deflections which reduce the angle of attack. When the vortex is convected past the trailing edge and the nose down pitching moment is diminished, the structure will tend to oscillate at the torsional natural frequency. If the time for the pitching moment change is equal to one half the torsional natural period of the blade, a powerful aeroelastic amplification of the blade pitch oscillation will occur. The changes in total lift will simultaneously interact with bending of the blade. These torsion and bending displacements must be included in a determination of the aerodynamic loads on the airfoil.

The time history of the movement of the pressure pulses has been defined by Carta (ref. 6). Pressures measured on a pitching airfoil were presented as pseudo-three-dimensional plots of pressure time histories (fig. 4). The ridges define regions of low pressure and the valleys define regions of higher pressures. The time history at each chordwise location has a peak. Connecting the peaks from leading to trailing edge defines a ridge. The slope of the ridge is related to the speed of a pressure pulse that proceeds from the leading to the trailing edge. The speed depends strongly on reduced frequency and to a lesser degree on the mean angle of attack. There is also some evidence that the speed depends on the amplitude of oscillation of angle of attack.

The time history of the pressure pulses becomes even more complex when plunging motion is considered. In a separate investigation (ref. 7), Carta found that plunge motion caused patterns in the pressures that were not observed in pitching motion. Figure 5 compares the phases of the first two harmonics of the pressures on the airfoil upper surface. Arrows have been added to Carta's figure to indicate that decreasing phase angle represents rearward movement of the pressure associated with the harmonic. Although this test was at a relatively low speed (Mach = 0.18 and Reynolds number = 0.6 x 10^6), it is clear that empirical approximations to vortex motion based on pitch alone are inadequate for the mixed pitch and plunge motions that occur on helicopter rotor blades. The downstream motion of vortices over pitching airfoils, although dependent on frequency and amplitude, is at least a smooth function of time. However, plunge motion apparently disrupts the orderly downstream propagation of vortices.

Recovery from Stall

The part of the dynamic stall cycle that is dominated by shed vortices is terminated by the recovery from stall. Once the airfoil aerodynamic angle of attack has decreased sufficiently to allow the flow over the airfoil upper surface to reattach, initially the process of vortex shedding will cease, then previously shed vortices will be convected downstream, and eventually the airfoil will become completely unstalled. This is the least investigated and most analytically intractable part of the dynamic stall cycle. An early investigation (ref. 8) showed that the recovery process was non-repeatable. Figure 6 shows both lift and pitching moment variations for successive cycles of an airfoil oscillating in pitch. The cause of the non-repeatability is unknown. The phenomenon is made amenable to the data reduction process by cycle averaging. A careful study by McAlister, Carr, and McCroskey in reference 9 showed that by averaging 50 cycles of oscillation (fig. 7) the repeatable features of the experimental pressure time histories are preserved accurately, and the random variations are suppressed. This technique is standard practice for parametric comparisons.

An attempt to gain insight into the flow field after the shed vortices have passed downstream was summarized in reference 10. The experiments measured the velocities about the center span of an aspect ratio 8 wing at about 19.5^0 angle of attack. These static stall results were obtained in two experiments which are identified as the high-Mach-number (M = 0.49) case and low-Mach-number (M = 0.148) case. The velocities above the airfoil in the low-Mach-number case (fig. 8) form a classical turbulent free shear layer. The velocity profiles (fig. 9) are matched with Gortler profiles using a spreading parameter taken from shear layer experiments with free jets (ref. 11). The solid line in figure 9 was calculated by the inviscid analysis of reference 12. The solid line is the track of the vortex sheet that the inviscid analysis used to approximate the free shear layer. The experimental center of the free shear layer, the dashed line, agrees with the analysis amazingly well. The high-Mach-number airfoil was found to shed strong vortices from near the airfoil crest (fig. 10). As these vortices were convected downstream the paths that successive vortices followed grew increasingly random as they approached the trailing edge. The convection speed increased from about 30% of the freestream speed near the crest to near the freestream speed at the trailing edge.

These experiments suggest that as the shed vortices in dynamic stall are convected downstream, a free shear layer is established behind them. This free shear layer is amenable to analysis because it tends in the steady state toward simple jet-like velocity profiles. However, the number and timing of the vortices shed from near the crest of the airfoil is not known.

Wake Vorticity

As the shed vortices move downstream, a large wake region is formed behind the airfoil. Information about the wake comes from low-Reynods-number flow visualizations and from measurements in static stall wakes. The inviscid static stall model of reference 12 does not require the vortex sheets shed from near the airfoil crest and from the trailing edge to meet downstream. Figure 9 shows a gap between the two vortex sheets calculated by Maskew and Dvorak. Through this gap fluid is convected forward into the separated region. This has been observed in the flow fluctuations made visible by the vapor screen technique illustrated in figure 11. Fluid is lost from the separated region by entrainment. Figure 12 is a detail of figure 9 showing the entrainment caused by the shear layer at the trailing edge. Because of this entrainment there can be no wake closure in static stall.

In dynamic stall the vorticity shed into the wake during one cycle can be as much as one-half of the bound vortex strength required to give the airfoil its maximum lift. Figure 6 shows the lift coefficient decreasing from 1.4 to 0.7 during the stall process. The change in circulation on the airfoil is of course equal to the circulation contained in the shed vortices. The velocity induced by a shed vortex will be a significant influence on the airfoil angle of attack even after it has been convected 20 or 30 chord lengths downstream. The very detailed flow visualizations of McAlister and Carr (ref. 13) show a thick wake even before stall occurs. During stall recovery (fig. 13) the shed vortices in the wake are convected far above the plane of the airfoil. Therefore, not only the distance downstream of the trailing edge but also the height of the vortex is significant. The position of the shed vortices, both distance downstream and vertical location, will be a strong influence on the airfoil upper surface pressure distribution.

Stall Triggers

Attached Flow

The many schemes available to calculate the flow about unstalled airfoils remain valid for dynamic stall only until the angle of attack becomes sufficiently large to cause disturbances in the boundary layer. The boundary layer is unsteady, and, at the Reynolds numbers of interest (about 1 to 8 million based on airfoil chord), it is laminar about the nose and turbulent at the trailing edge. Four boundary layer phenomena have been identified as potential triggering mechanisms for the shedding of vortices. The mechanisms are:

1. Bursting of a bubble of separated flow that forms at moderate angles of attack on the airfoil upper surface at the boundary layer transition point.
2. The arrival at the leading edge region of a turbulent boundary layer flow reversal point that is moving forward from the trailing edge.
3. Shock wave-boundary layer interaction behind the airfoil crest.
4. Acoustic waves underneath the airfoil propagating from the trailing edge upstream near the airfoil lower surface and perturbing the stagnation and flow separation points.

The initiation of the vortex shedding process may involve more than one of these mechanisms. The mechanism that first succeeds in triggering vortex shedding will depend on airfoil shape, Mach and Reynolds numbers.

The ability to predict boundary layers is a necessary starting point for a dynamic stall analysis because all the triggering mechanisms involve the attached boundary layer to some extent. Although steady boundary layers (excluding shock interaction) are predictable, there are few theories and less data for unsteady turbulent boundary layers. A vigorous research program is being conducted at the U. S. Army Research and Technology Laboratory by L. W. Carr to define the characteristics of unsteady boundary layers and boundary layer separation.

Flow Reversal and Separation

The first stall trigger to be considered is the bursting of the separation bubble. For many airfoils the process of transition from laminar to turbulent boundary layer flow is carried out in a separation bubble. The bubble begins at the separation point of the laminar boundary layer. At low angles of attack, the zone of flow separation remains small, and the flow above the separation zone changes from laminar to turbulent. The onset of turbulence will, in moderately adverse pressure gradients, allow the boundary layer to reattach and close the separation bubble. If the pressure gradient is so adverse that the flow cannot reattach, or if the displacement thickness grows so rapidly that the transition to turbulence is too far from the airfoil surface to reattach the boundary layer, then the bubble is said to have burst. The bursting is characterized by massive separation and vortex shedding. The displacement thickness of the separation bubble tends to alleviate the pressure gradient, making it less adverse. Figure 14 is taken from an early study by Shamroth and Kreskovsky (ref. 14) that ignored the pressure gradient alleviation in calculating the separation bubble. The bubble grew far beyond a reasonable value without any bursting phenomena being manifested. This anomaly was explained by experimental measurements using hot films on the airfoil upper surface by Carr, McAlister and McCroskey (ref. 15) and by an analytical study by Scruggs, Nash, and Singleton (ref. 16). These two works identified the second stall trigger.

The second stall trigger is the flow reversal movement in the turbulent boundary layer on the airfoil upper surface. The progressive separation of the turbulent boundary from trailing edge to leading edge as the angle of attack increased is a common cause of stall in quasi-steady experiments. This behavior is illustrated in figure 15. For the dynamic case the pitch rate affects both the potential flow and the turbulent boundary layer. Both unsteady effects retard the forward movement of the separation point. However, once forward movement began, the speed calculated by this incompressible analysis could exceed sonic speed for practical helicopter applications. Furthermore, the analysis showed that even though the flow near the wall was in the upstream direction, the viscous region remained thin and caused little disturbance in the pressure distribution. This flow reversal without massive separation is short-lived. Experiments showed that vortex shedding was soon initiated. The means of interaction between the flow reversal in the turbulent boundary layer and the separation bubble is not known but flow reversal has been found to precede vortex shedding for most of the airfoils tested. Thus the separation of the compressible, turbulent, unsteady boundary layer, and the transition in the separation bubble are important mechanisms in the initiation of dynamic stall.

Mach-dependent Stall Initiation

The last two stall triggers are deduced from stall initiation observed in static stall. Schlieren flow visualizations, such as figure 16 from reference 17 have not yet been obtained for dynamic stall. Even though supersonic flow over the airfoil crest has been achieved for a freestream Mach number near 0.3, the results of reference 4 show no shock wave formation. The influence of Mach number on the performance of an airfoil undergoing dynamic stall has been well documented (ref. 18), but the role of a shock in stall initiation has not.

Another possible, but unproven, stall trigger mechanism was identified in static stall by St. Hilaire, Carta, Fink and Jepson in reference 19. A meticulous scrutiny of the airfoil surface pressures (fig. 17) revealed that identifiable pulses in the pressure time histories were moving upstream on the airfoil lower surface. The speed of movement roughly coincided with the sonic speed minus the local flow velocity. The pulses were observed to move through the stagnation with a 180° phase shift and to go around the nose of the airfoil. Vortex shedding was usually preceded by the arrival of a pressure pulse, although not all pulses triggered vortex shedding. This phenomenon must depend strongly on free stream Mach number. Thus the compressibility of the flow both inside and external to the viscous regions is an important fluid flow mechanism because both shock waves and acoustic waves have the potential of triggering vortex shedding.

Yaw Effects

Helicopter blades are in a yawed flow because of the combination of rotational and forward flight velocities. The yaw angle varies from a typical value of $+30^{\circ}$ (blade over the tail) to -30° (blade over the nose). A recent experimental study (ref. 19) provided the first evaluation of yaw effects on dynamic stall. The yawed flow was simulated by a swept, tunnel-sparning wing. The wing was oscillated in pitch about the quarter chord. Two yaw angles, 0° and 30°, and two Mach numbers, 0.30 and 0.40 were tested. Preliminary data reduction, consisting of only the overall lift and moment, has revealed quantitative changes in the dynamic stall behavior, but as yet no flow mechanism unique to yawed flow has been identified. Thus it is tentatively concluded that the two-dimensional flow characteristics discussed in the previous sections also control yawed dynamic stall. However, several results lead to the conclusion that the yaw will modify the dynamic stall flow phenomenon.

Figure 18 summarizes the effect of yaw on the airfoil pitching moment during a dynamic stall oscillation. The delay of the beginning of stall is indicative of boundary layer changes. The decrease in the rate of change of moment after stall may be associated with changes in the strength and convection speed of shed vorticity. The smaller minimum pitching moment could be caused by the shedding of multiple vortices over a longer period of time. Detailed examination of the pressure distributions is now underway to define the causes of the yaw effects. At this time a two-dimensional airfoil model appears to be a prerequisite for yawed flow calculations.

Aeroelastic Evaluation

Flow Phenomena and Structural Response

The structural responses that affect the flow in dynamic stall have been discussed in previous sections. The flow phenomena that are most important in determining the structural response will be summarized in this section. In order to define a complete flow model the manner in which the flow model might be utilized in the context of the aeroelastic interactions is briefly discussed.

The pressure distribution on airfoils in static stall has been satisfactorily predicted by a combination of attached boundary layer calculations and an inviscid model with free shear layers. All static stall models are explicitly steady state in that the spontaneous shedding of vortices, such as those shed from a circular cylinder, are excluded from consideration. For dynamic stall the calculation of the shedding mechanism is essential, but the shedding of at least the initial vortex should be much easier to predict than spontaneous shedding in static stall. The list of possible triggering mechanisms will probably be reduced by additional experiments but at least three fluid flow mechanisms must be considered: (1) a separation bubble near the leading edge that begins at the laminar boundary layer separation point and ends in a turbulent reattached boundary layer, (2) a compressible, unsteady, turbulent boundary layer on both the upper and lower airfoil surfaces, (3) shock or sonic wave interaction with the boundary layer. Immediately after stall onset, a large shed vortex is convected over the airfoil upper surface. Laminar calculations for pitch

motion show that the vortex shape and speed are strongly influenced by its close proximity to the airfoil upper surface. The process by which secondary vortices are shed, although calculable for laminar flow, may have a different trigger mechanism from the initial shed vortex. Certainly the pressure patterns on the upper surface of a plunging airfoil suggests a more complex pattern of vortex shedding and movement than in pitching motion. The reattachment of the flow and the formation of attached boundary layers is nonrepeatable from cycle to cycle. Speculative extrapolation from static stall suggests that free shear layers may form above the airfoil upper surface and behind the trailing edge before the flow reattaches.

For calculations applicable to helicopters the relative importance of various aerodynamic characteristics is controlled by the interaction with the blade structure. It is most important to calculate a time-accurate history of the pitching moment. Unlike classical flutter, in which a free structural response is driven by negative aerodynamic damping, the blade motion in dynamic stall is primarily a few cycles of forced response in torsion. Thus the strength and location of the shed vortex must be calculated accurately. The lift controls the blade bending and flapping. The structural response in these two modes is much slower than the torsional response and the resulting motions have less effect on angle of attack. Thus the airfoil lift is secondary in importance to the pitching moment. Since stall occurs when the blade is on the retreating side of the rotor disk, the drag increases the propulsive force of the rotor. This offsets the detrimental effect of drag on rotor shaft power sufficiently to make the drag of tertiary importance. The newer rotors have significant dynamic responses in the chordwise or lead-lag direction, but there is not yet a requirement for accurate calculation of drag time histories.

Flow Modeling

The uses to which a flow model might be put is one of the factors that determine the degree of completeness of the model needed. The lack of experimental measurements in the flow field puts severe demands on any analytical model of dynamic stall. The model must include the flow phenomena that can reasonably be expected to occur without the usual guidance of quantitative experiments. In fact, one of the major needs for analytical calculations is to guide experiments. Although a model that is sufficiently complete to use with confidence at this time will not be efficient enough for rotor aeroelastic calculations, three continuing needs for the best possible analysis are foreseen. New airfoil designs or boundary layer control devices which may change the stall trigger mechanism should first be analyzed by theory which contains all the possible trigger devices. Extensions of the theory beyond two-dimensional flow is most safely done with a complete model. Finally, the increasing expense of wind-tunnel experiments justifies the most complete model for guidance of the tests. Careful experiments, and not just a complete analytical model, should be available to measure the accuracy of the simpler and cheaper analyses that are needed for rotor performance and aeroelastic calculations.

Based on these requirements and the present knowledge of flow phenomena, a complete model of airfoil dynamic stall must account for the following flow phenomena:

1. A compressible laminar boundary layer with a moving separation point or transition point.

2. A separation bubble with possible transition to turbulence.

3. A turbulent, compressible, unsteady boundary layer with moving separation and with flow reversal in the thin viscous layer.

4. Shock wave interaction with the boundary layer.

5. The shedding of vorticity from the boundary layer separation or shock wave.

6. The movement of shed vorticity due to convection, diffusion, and shear forces.

7. Free shear layers above the airfoil upper surface and behind the trailing edge.

8. Induced velocities from previously shed vortices in a compressible free stream flow.

9. Acoustic wave propagation below the airfoil.

10. Arbitrary airfoil motion in pitch and plunge.

Concluding Remarks

The fluid flow mechanisms which have been identified include both proven and potential factors to be included in the analysis of helicopter blade dynamic stall. The uncertainties in the list of mechanisms are primarily due to the lack of flow field measurements in the pertinent ranges of Mach and Reynolds numbers. Until further experimental results are available the most promising means of testing the importance of an item on the list is a theoretical calculation that includes all the identified phenomena.

References

[1]Crimi, Peter, "Analysis of Helicopter Rotor Blade Torsional Oscillations Due to Stall," NASA CR-2573, September 1975.

[2]Crimi, Peter, "Analysis of Stall Flutter of a Helicopter Rotor Blade," NASA CR-2322, November 1973.

[3]McCroskey, W. J., "Some Current Research in Unsteady Fluid Dynamics," The 1976 Freeman Scholar Lecture, Journal of Fluids Engineering, vol. 99. (Also Transactions of the ASME, March 1977).

[4]McCroskey, W. J.; McAlister, K. W.; Carr, L. W.; Pucci, , S. L.; Lambert, O.; and Indergand, Lt. R. F. "Dynamic Stall on Advanced Airfoil Sections," Presented at the 36th Annual Forum of the American Helicopter Society, Washington, DC, May 1980, AHS Preprint 80-1.

[5]Mehta, Unmeel B., "Dynamic Stall of an Oscillating Airfoil," Presented at the AGARD Fluid Dynamics Panel Symposium on Unsteady Aerodynamics, Ottawa, Canada, September 1977, AGARD CP-227, Paper No. 23.

[6]Carta, Franklin O., "Analysis of Oscillatory Pressure Data Including Dynamic Stall Effects," NASA CR-2394, May 1974.

[7]Carta, F. O., "A Comparison of the Pitching and Plunging Response of an Oscillating Airfoil," NASA CR-3172, October 1979.

[8]Gray, Lewis; Liiva, Jaan; and Davenport, Franklyn J., "Wind Tunnel Tests of Thin Airfoils Oscillating Near Stall. Volume I: Summary and Evaluation of Results," USAAVLABS Technical Report 68-89A, January 1969.

[9]McAlister, Kenneth, W.; Carr, Lawrence W.; and McCroskey, William, J., "Dynamic Stall Experiments on the NACA 0012 Airfoil," NASA TP-1100, January 1978.

[10]Young, Warren H., Jr.; and Hoad, Danny R., "Comparison of Two Flow Surveys Above Stalled Wings," AIAA Paper 79-0147, January 1979.

[11]Birch, S. F.; and Eggers, J. M., "A Critical Review of the Experimental Drag for Developed Free Turbulent Shear Layers," NASA SP-321, Conference on Free Turbulent Shear Flows, July 1972, pp. 11-37.

[12]Maskew, B.; and Dvorak, F. A., "The Prediction of $C_{l_{max}}$ Using a Separated Flow Model," Journal of the American Helicopter Society, vol. 23, April 1978, pp. 2-8.

[13]McAlister, Kenneth W.; and Carr, Lawrence W., "Water-Tunnel Experiments on an Oscillating Airfoil at Re = 21,000," NASA TM-72446, March 1978.

[14]Shamroth, S. J.; and Kreskovsky, J. P., "A Weak Interaction Study of the Viscous Flow About Oscillating Airfoils," NASA CR-132425, May 1974.

[15]Carr, Lawrence W.; McAlister, Kenneth W.; and McCroskey, William J., "Analysis of the Development of Dynamic Stall Based on Oscillating Airfoil Experiments," NASA TN D-8382, January 1977.

[16]Scruggs, R. M; Nash, J. F.; and Singleton, R. E., "Analysis of Dynamic Stall Using Unsteady Boundary-Layer Theory," NASA CR-2462, October 1974.

[17]Ladson, Charles L., "Description and Calibration of the Langley 6- by 19-inch Transonic Tunnel," NASA TN D-7182, May 1973.

[18]Gray, Lewis; and Liiva, Jaan, "Two-Dimensional Tests of Airfoils Oscillating Near Stall, Volume II: Data Report," USAAVLABS Technical Report 68-13B, April 1968.

[19]St. Hilaire, A. O.; Carta, F. O.; Fink, M. R.; and Jepson, W. D., "The Influence of Sweep on the Aerodynamic Loading of an Oscillating NACA 0012 Airfoil. Volume I: Technical Report," NASA CR-3092, May 1979.

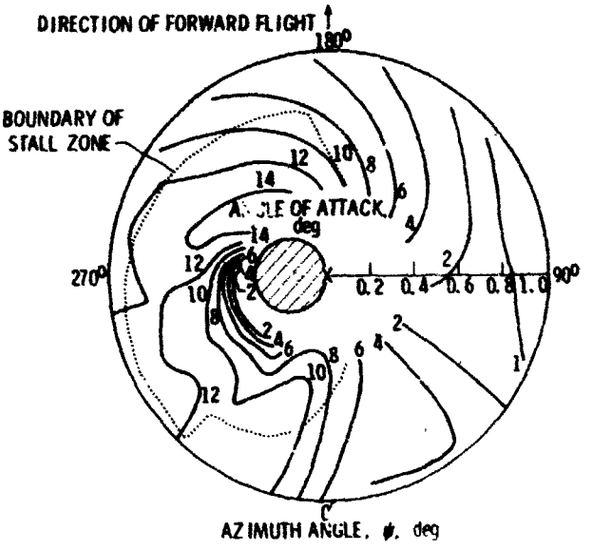

Fig. 1 Computed angle of attack distribution and stall zone for helicopter rotor disk (ref. 1).

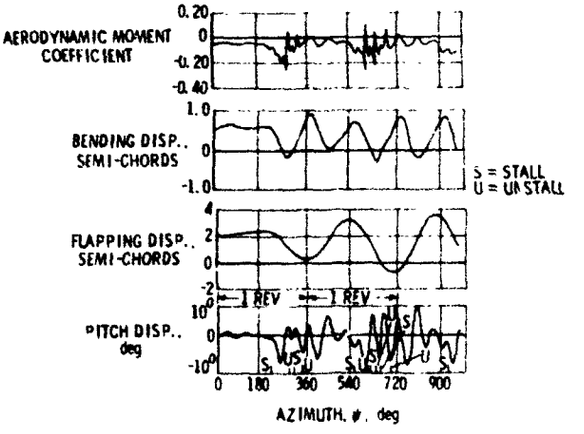

Fig. 2 The interaction of dynamic stall and helicopter blade motions (ref. 1).

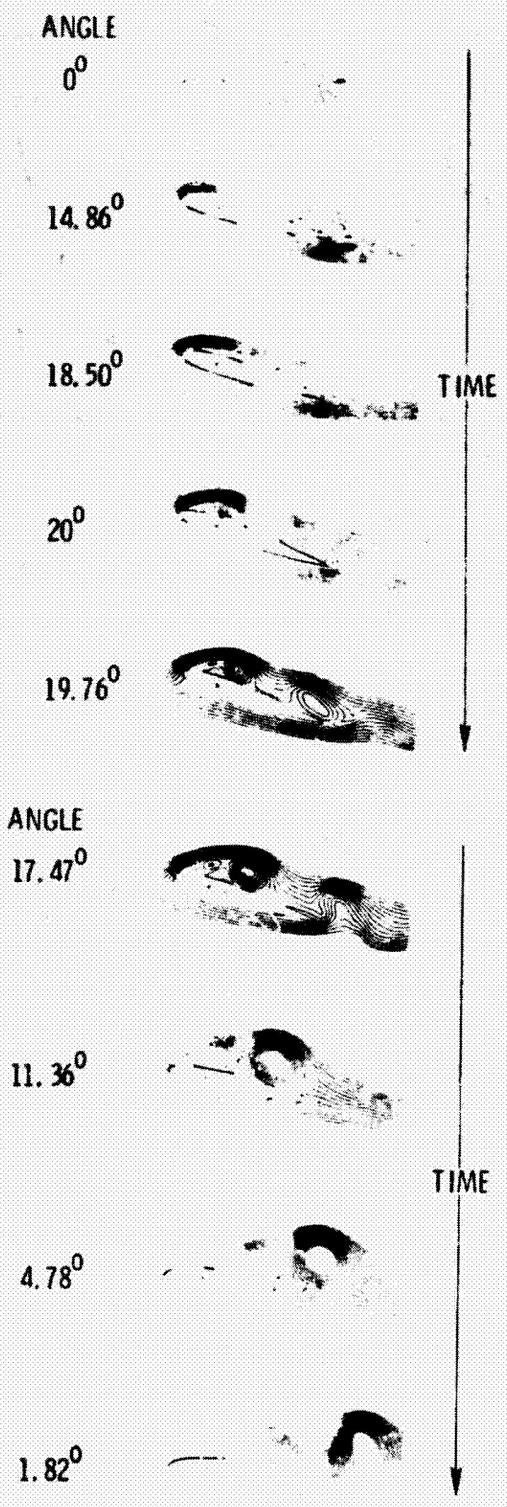

Fig. 3 Calculation of streamlines for one cycle of dynamic stall in laminar flow (ref. 5)

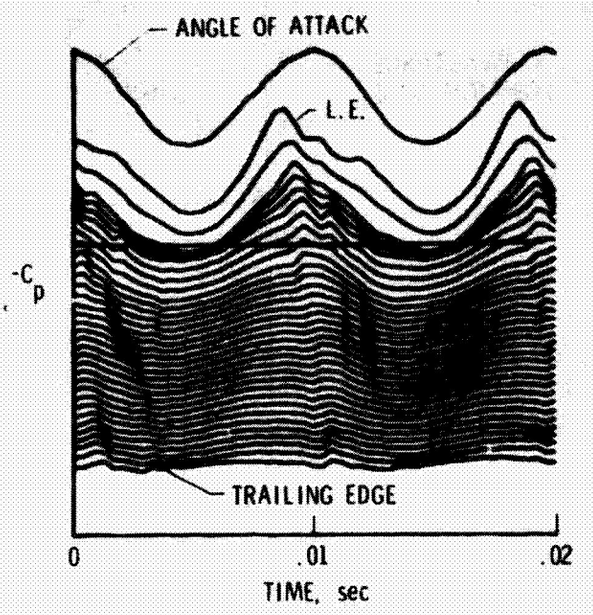

Fig. 4 Time histories of airfoil pressures in a pseudo-three-dimensional format (ref. 6).

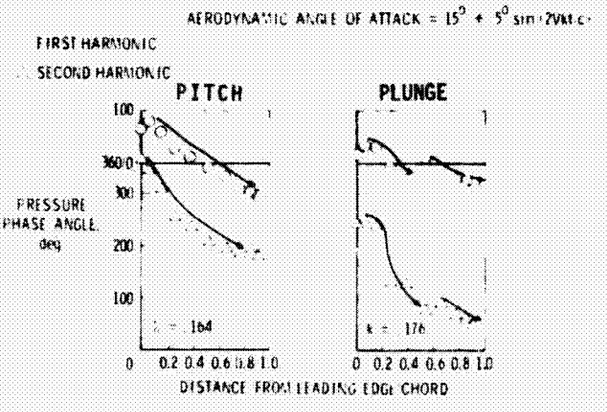

Fig. 5 Phase angles of pressure harmonics for airfoil dynamic stall (ref. 7).

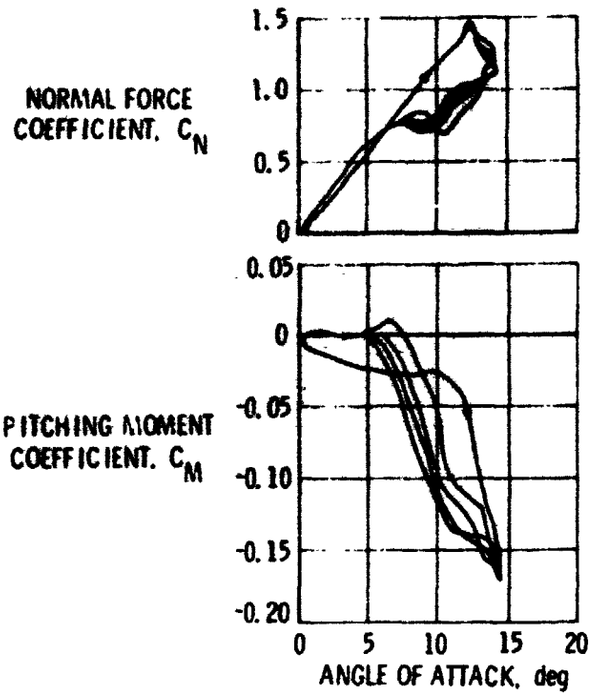

Fig. 6 Successive cycle-to-cycle variations in C_N and C_M during pitch oscillations (ref. 8).

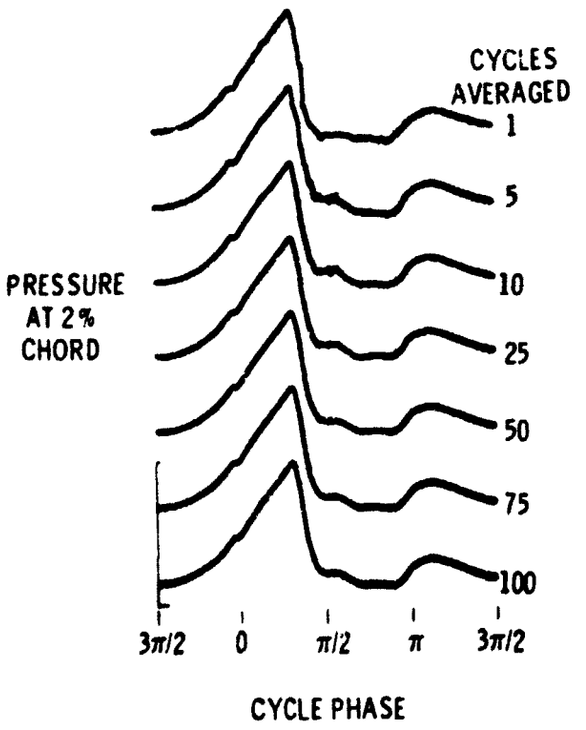

Fig. 7 Effect of cycle averaging on surface pressure for dynamic stall oscillations (ref. 9).

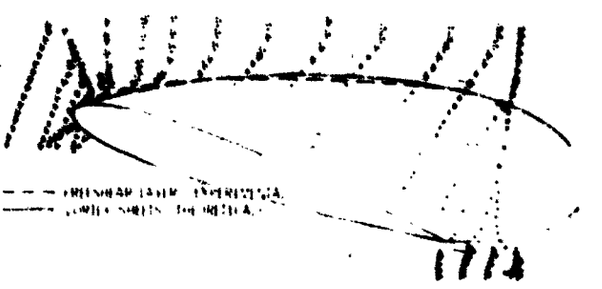

Fig. 8 Measured velocities and correlation of free shear layer locations for low-Mach-number case (ref. 10).

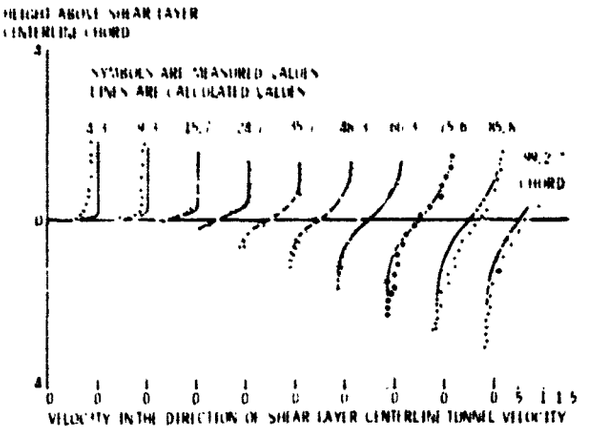

Fig. 9 Measured velocities above a stalled airfoil compared to turbulent free shear layer profiles (ref. 10).

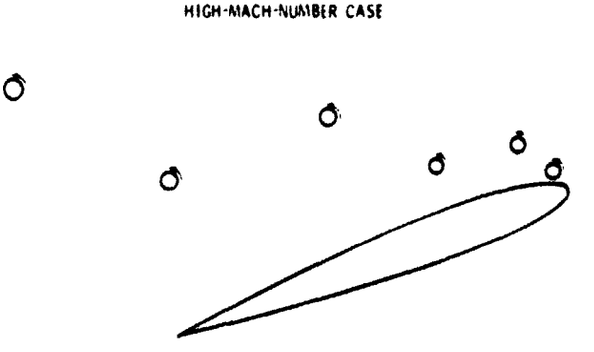

Fig. 10 High-Mach-number case concept of shed vortices (ref. 10).

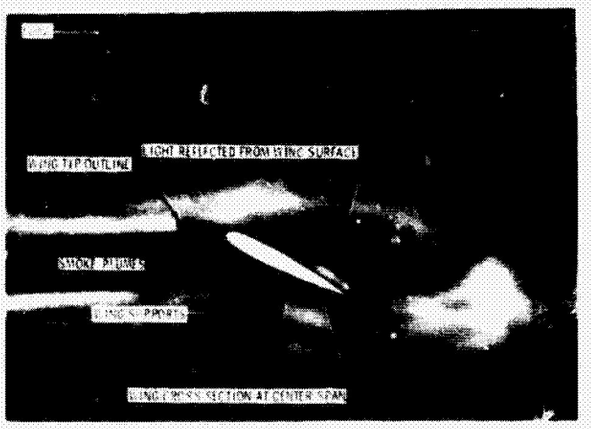

Fig. 11 Smoke flow visualization at the wing center span in static stall (ref. 10).

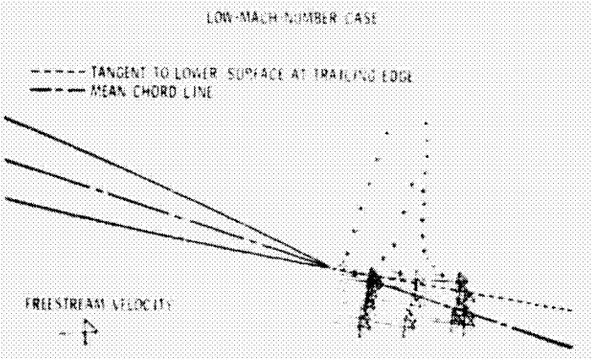

Fig. 12 Resultant mean velocity vectors behind the trailing edge of a stalled airfoil (ref. 10).

Fig. 13 Water tunnel flow visualization of recovery from stall of an oscillating airfoil (ref. 13).

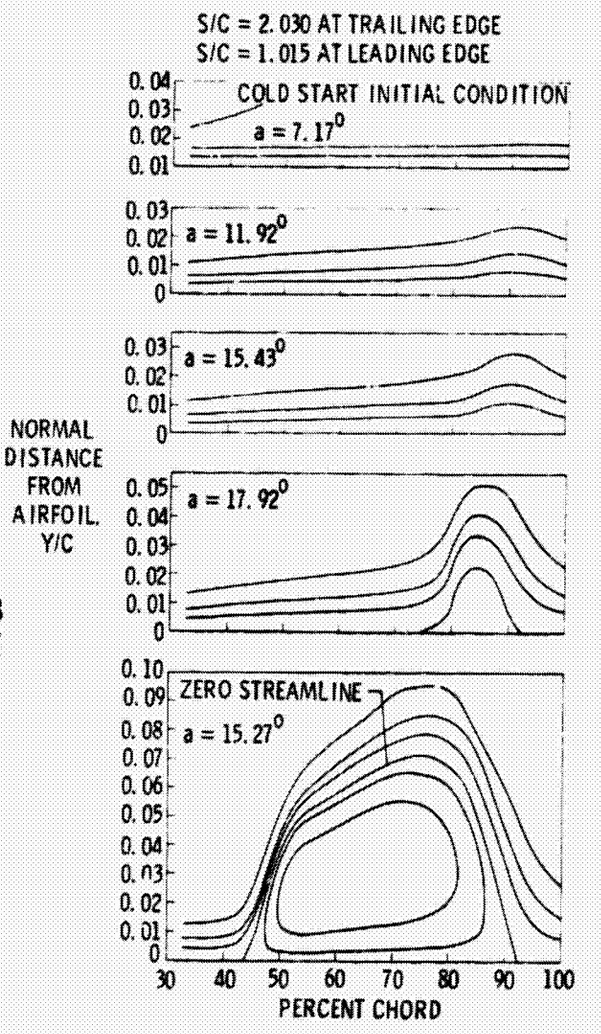

Fig. 14 Calculated streamlines about a leading edge bubble for an oscillating airfoil (ref. 14).

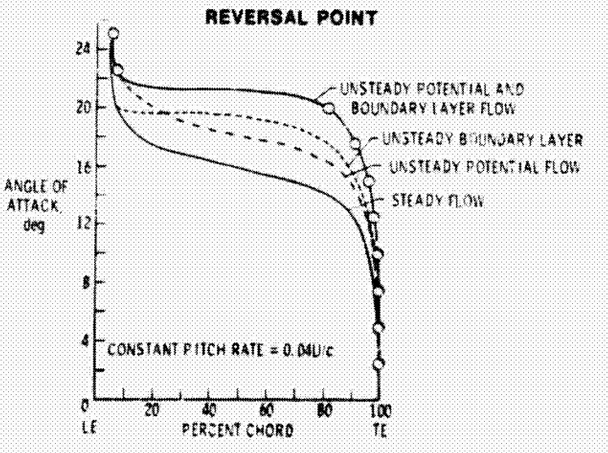

Fig. 15 Movement of the boundary layer flow reversal point on an airfoil pitching from 0° to 25° angle of attack (ref. 16).

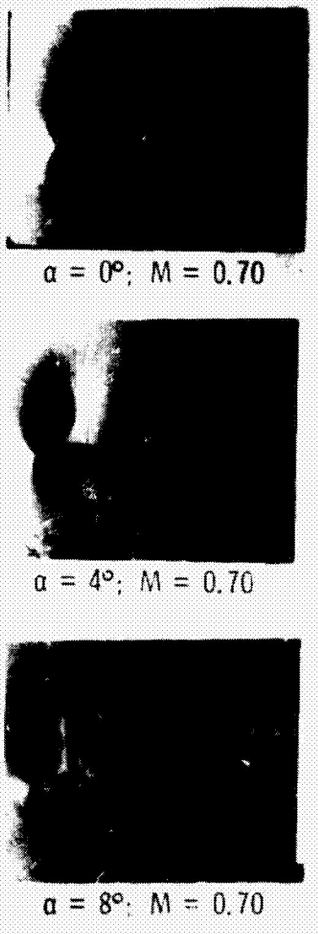

Fig. 16 Schlieren visualization of shock induced separation in steady flow (ref. 17).

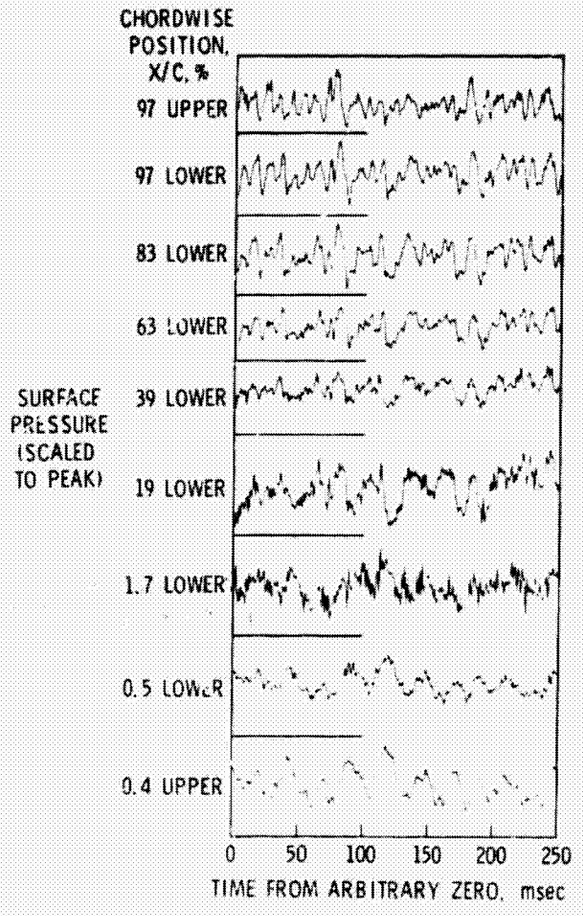

Fig. 17 Pressure time histories on the surface of an airfoil at 15° angle of attack (ref. 19).

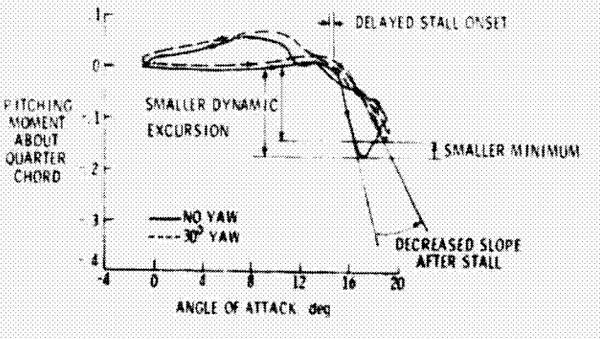

Fig. 18 The effect of yaw angle on an airfoil oscillating in pitch (ref. 19).